Clinical Plasma Medicine 17–18 (2020) 100092

Contents lists available at ScienceDirect

Clinical Plasma Medicine

journal homepage: www.elsevier.com/locate/cpme

Original research article

Magnetic field enhanced cold plasma sterilization

Madeline A. Mackinder[a], Keliang Wang[a,b], Bocong Zheng[a,b], Maheshwar Shrestha[a,b], Qi Hua Fan[a,b,*]

[a] Department of Chemical Engineering and Material Science, Michigan State University, East Lansing, MI 48824, United States
[b] Department of Electrical Engineering & Computer Engineering, Michigan State University, East Lansing, MI 48824, United States

ARTICLE INFO

Keywords:
Plasma
Sterilization
Magnetic field

ABSTRACT

Cold plasma sterilization offers an efficient way to sterilize medical components and instruments. This paper reports using a magnetized plasma to realize low-temperature sterilization. A radio frequency dielectric barrier discharge is created in a quartz tube using a mixture of argon and oxygen gas. A uniform amount of *Escherichia coli* is applied onto glass slides and exposed to the plasma afterglow at different pressures with and without a magnetic field. Optical emission spectroscopy is used to identify the plasma species present. The magnetic field significantly promotes the intensity of the plasma and the sterilization efficiency. A process gas pressure of 100 mTorr presents the most effective treatment with a sterilization time less than one minute and sample temperature below 32 °C.

1. Introduction

Sterilization is a physical or chemical process that exterminates or inactivates microorganisms [26]. The worldwide accepted definition for medical devices to be considered sterile is the security assurance level (SAL) [18]. The SAL is a statistical parameter that refers to the probability of one surviving viable microorganism after sterilization [18]. For medical devices, SAL needs to be below 10^{-6}, meaning 1 in 1,000,000 chance [18].

Sterilization plays a major role in health-care facilities to prevent the spread of disease. Current sterilization methods include using autoclave or heat, ethylene oxide gas, hydrogen peroxide gas plasma, and radiation [26,31]. These sterilization methods have their limitations. The use of an autoclave or heat is not advisable for heat-sensitive materials because they may be disfigured [31]. Ethylene oxide can be used for heat-sensitive materials, but it presents a risk in its toxicity [31]. Surfaces treated with ethylene oxide require an airing time before they are safe to handle [22]. The use of hydrogen peroxide also requires a long processing time and a long ventilation time [22]. Gamma rays have been used in radiation sterilization [31]. Using radiation requires protection for the operators and a special site to perform it [31]. Plasma sterilization presents an option that is low temperature, efficient, and non-toxic.

The existing hydrogen peroxide gas plasma process is 'partially' plasma sterilization [30]. This process includes two phases: a diffusion phase and a plasma phase [15,26,30]. First, the sterilization chamber is evacuated, and hydrogen peroxide solution is injected from a cassette and is vaporized in the sterilization chamber. The hydrogen peroxide vapor diffuses through the chamber and initiates the inactivation of microorganisms on all the surfaces exposed to the sterilant. Second, a gas plasma is created in the chamber. The residual hydrogen peroxide is then broken apart by the plasma, which aids in the removal of hydrogen peroxide residuals from the sterilizer load in order to make the contents safe for handling and use. Hence, the hydrogen peroxide plasma treatment is a direct gas plasma sterilization.

In the past 15 years, low-temperature pure gas plasma sterilization has attracted great interest because of the unique characteristics of plasmas. Plasma is quasi-neutral ionized gas, known as the fourth state of matter. A large number of gas ions (e.g. O_2^+), atoms (e.g. O), and excited species (e.g. O*, O_2*) can be created in a plasma. These gas species are highly reactive and can effectively destroy or inactivate bacteria. Current literature agrees that there are three mechanisms by which plasma sterilizes a surface: ultra-violet (UV) irradiation of genetic material, chemical reactions with the plasma species, and plasma ion sputtering [4].

Previous studies have shown that the reactive species and ions created in plasmas play the largest role in sterilization. Hence, a high plasma density is expected to promote sterilization efficiency. One aspect of this work is to understand the effects of gas pressure on sterilization efficiency because a plasma density is directly affected by the gas pressure. On the other hand, an increased plasma density usually leads to large heating load to the working piece surface due to the

* Corresponding author.
E-mail address: qfan@egr.msu.edu (Q.H. Fan).

https://doi.org/10.1016/j.cpme.2019.100092
Received 14 March 2019; Received in revised form 10 October 2019; Accepted 17 October 2019

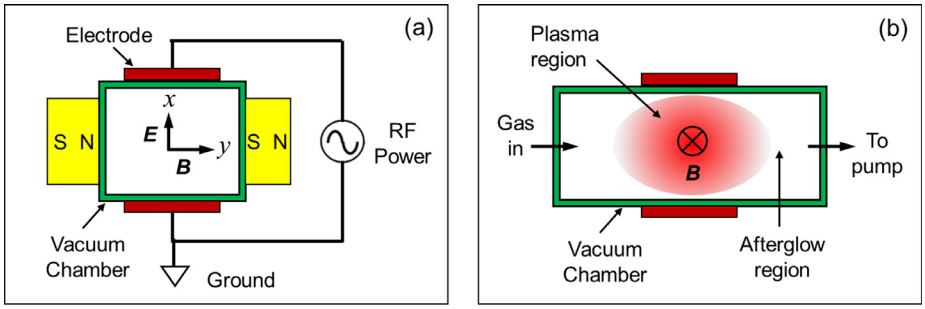

Fig. 1. Schematic diagram of the plasma reactor setup. a) Profile view. b) Side view.

bombardment of the charged particles created in the plasma. Hence, another aspect of this work is to reduce the heating load to the sample surface by integrating a magnetic field to confine the plasma. This research combines plasma modeling with optical emission spectroscopy to verify the effects of a magnetic field on the concentrations of plasma species. Subsequently, the sterilization efficiency and temperature with the use of a magnetized plasma are determined. The plasma modeling also helps to predict the reactive species that play an essential role in sterilization.

2. Experimental and theoretical methods

2.1. Plasma system and process

A dielectric barrier discharge plasma system was used for sterilization experiments. The schematic of the setup is shown in Fig. 1. A quartz tube was used as a vacuum chamber and was connected to a mechanical pump, pressure gauge, and a gas flow controller. A pair of electrodes was used to generate plasmas. One of the electrodes was connected to a radio frequency (RF) power generator through a matching network. The operation frequency was 13.56 MHz. The other electrode was grounded. A magnetic field was created by a permanent magnet assembly (Fig. 1). The magnetic field in the plasma region was generated in a direction perpendicular to the electrical field or in parallel to the electrode surface. A glass slide inoculated with the bacterial sample was placed on a boat and set at a downstream position right beyond the electrode (plasma) region, noted as the afterglow region. The magnetic field effectively confines energetic electrons from reaching the sample. Hence, using the afterglow region for sterilization is expected to further lower the process temperature as compared to using the direct plasma region.

Before igniting a plasma, the quartz tube was evacuated with the vacuum pump to $<1 \times 10^{-2}$ Torr and purged with the process gas 5 times to prevent cross contamination. The tube was subsequently filled with the process gas, e.g. a 10% O_2–90%Ar mixture. The gas flow was adjusted by a mass flow controller to achieve a test pressure. Then the RF power was turned on and the matching network was adjusted to reach a zero-watt reflection power. The RF power was maintained at 70 W through all experiments.

The temperature studies were performed in triplicate for the direct and afterglow areas, and with and without a magnetic field. Temperature was measured using an infrared thermometer (Fluke 572–2 High Temperature Infrared Thermometer, Fluke Corporation, USA). To keep measurements consistent, the thermometer was held in place by attaching it to a ring stand with a clamp.

2.2. Modeling of magnetically enhanced plasma discharges

A volume-averaged global model is developed to evaluate the magnetically enhanced dielectric barrier discharges, which can provide a description of plasmas with complex chemistry set without the intensive computation required for spatially resolved models. The aim of using global model here is to quickly predict spatially averaged plasma parameters such as densities of each species that would otherwise be difficult to simulate and diagnose. Since the qualitative change of the plasma parameters with the process parameters is the primary goal of this model research, the specific values of the plasma parameters are less important, this makes the global model the best choice here. The structure of the system is illustrated in Fig. 1. The plasma generated in the quartz tube diffuses and loses isotropically to the inner walls of the tube. However, by applying a strong magnetic field in y direction to the discharge system, the charged species and power losses perpendicular to the magnetic field are significantly suppressed. Due to the reduced effective loss area of mass and energy, the electron density, as well as the number densities of reactive species, are expected to be increased. In that case, the influence of the magnetic field should be considered in the model, as described as follows.

First, consider the case of no magnetic field. The mass balance equation for heavy species is

$$\frac{\partial n_k}{\partial t} = R_k + \frac{1}{V}\sum_s A_s \Gamma_{k,s}, \tag{1}$$

where n_k is the number density of species k, t the time, $R_k = \sum_k k_{iz,k} n_k n_e$ the reaction rate, $k_{iz,k}$ the ionization rate coefficient of electron collisions with species k (see Table 1), n_e the electron density, $V = 7.8\ cm^3$ the reactor volume, $A_s = 12.5\ cm^2$ the surface area. The flux of ion species k at a surface s is $\Gamma_{k,s} = \frac{\gamma_k}{1-\gamma_k/2}\frac{1}{4} n_k \sqrt{\frac{8k_B T_k}{\pi m_k}}$, where k_B is the Boltzmann constant, $\sqrt{8k_B T_k/\pi m_k}$ the averaged thermal velocity, $\gamma_k = 1$ the sticking coefficient, $T_k = 400\ K$ the temperature and m_k the mass of heavy species k. Assuming the plasma is quasi-neutral, the electron density is

$$n_e = \sum_k z_k n_k, \tag{2}$$

where z_k is the charge number of species k. The energy balance equation is

$$e\frac{\partial n_\varepsilon}{\partial t} = \frac{P_{abs}}{V} + R_\varepsilon + \frac{1}{V}\sum_s \sum_{pi} eA_s \Gamma_{k,s}(\varepsilon_e + \varepsilon_i), \tag{3}$$

where e is the elementary charge, n_ε the electron energy density, $P_{abs} = 70W$ the absorbed power, $R_\varepsilon = e\sum_K k_k n_k n_e \Delta\varepsilon_k$ the electron energy variation due to polarization scattering and inelastic collisions, k_k and $\Delta\varepsilon_k$ are the rate coefficient and the energy variation between electron and species k (see Table 1), $\varepsilon_e = 2T_e$ and $\varepsilon_i = \frac{1}{2}T_e + V_s$ are the mean kinetic energy lost per particle lost for electrons and ions, respectively [19]. T_e is the electron temperature and V_s is the potential drop across the sheath. The last term on the right-hand side of the above equation is summed over all surfaces and all positive ions.

Without an external magnetic field, the generated plasma contacts with the inner surface of the dielectric tube in x and y directions and flows outward freely in z direction. Assuming the center-to-edge density ratio of ions is h_s, the flux of ion species j can be expressed as $\Gamma_j = h_s n_j u_{B,j}$, where $u_{B,j}$ is the Bohm velocity of ion species j. From an

Table 1
Principal rate coefficients used in the model.

Reaction	Rate coefficient (m^3/s)	Threshold (eV)	Reference
$e + Ar \rightarrow e + Ar$	$2.336 \times 10^{-14} T_e^{1.609} \times \exp(0.0618(\ln T_e)^2 - 0.1171(\ln T_e)^3)$		[19]
$e + Ar \rightarrow 2e + Ar^+$	$2.34 \times 10^{-14} T_e^{0.59} \exp(-17.44/T_e)$	15.76	[9]
$e + Ar \rightarrow e + Ar^m$	$2.5 \times 10^{-15} T_e^{0.74} \exp(-11.56/T_e)$	11.56	[17]
$e + Ar^m \rightarrow e + Ar$	$4.3 \times 10^{-16} T_e^{0.74}$	−11.56	[1]
$e + Ar^m \rightarrow 2e + Ar^+$	$6.8 \times 10^{-15} T_e^{0.67} \exp(-4.2/T_e)$	4.2	[13]
$e + O \rightarrow 2e + O^+$	cross section	13.61	[16]
$e + O_2 \rightarrow e + O_2(a)$	cross section	0.977	[3,11]
$e + O_2 \rightarrow 2e + O_2^+$	cross section	12.06	[11]
$e + O_2 \rightarrow e + 2O$	cross section	13.5	[6]
$e + O_2 \rightarrow O^- + O$	cross section	4.3	[12]
$e + O_2(a) \rightarrow e + 2O$	cross section	12.523	[8]
$O + O^- \rightarrow e + O_2$	1.5×10^{-16}		[8]
$O + 2O_2 \rightarrow O_3 + O_2$	$6.4 \times 10^{-47} \exp(663/T_g)$		[8]
$O + O_2 + O_3 \rightarrow 2O_3$	$1.3 \times 10^{-46} \exp(663/T_g)$		[8]
$O + O_2^- \rightarrow O^- + O_2$	$1.5 \times 10^{-16} (T_g/300)^{0.5}$		[8]
$O + O_2^- \rightarrow e + O_3$	1.5×10^{-16}		[8]
$O + O_3 \rightarrow 2O_2$	$8 \times 10^{-18} \exp(-2060/T_g)$		[8]
$O^- + O_2 \rightarrow O + O_2^-$	1×10^{-16}		[8]
$O^- + O_2^+ + M \rightarrow O + O_2 + M$	$2 \times 10^{-37} (T_g/300)^{-2.5}$		[8]
$O_2(a) + O_3 \rightarrow 2O_2 + O$	1×10^{-20}		[8]

intermediate pressure of 50 mTorr to a high pressure of 1 Torr, the center-to-edge ratio can be expressed as

$$h_l \approx \frac{0.86}{[3 + l/2\lambda_i + (0.86 l u_B/\pi D_a)^2]^{1/2}} \quad (4)$$

at the axial sheath edge and

$$h_R \approx \frac{0.8}{[4 + R/\lambda_i + (0.8 R u_B/\chi_{01} J_1(\chi_{01}) D_a)^2]^{1/2}} \quad (5)$$

at the radial sheath edge, respectively [19]. $l = 5\ cm$ and $R = 1.25\ cm$ are the length and radius of the cylindrical reactor, $\lambda_i = \frac{1}{n_g \sigma}$ is the mean free path of ions, n_g the number density of background gas and σ the cross section of ion-neutral collisions, $D_a \approx \mu_i T_e$ is the ambipolar diffusion coefficient, $\mu_i = z_i e/m_i \nu_m$ is the ion mobility, m_i is the ion mass and ν_m is the momentum transfer frequency, J_1 is the first-order Bessel function and χ_{01} is the first zero of the J_1 Bessel function. In x direction, there are high-voltage sheaths on the dielectric surface, which we assume is about $V_s \approx$ 1000V. The neutral species α diffuses to the walls isotropically with a flux of $\Gamma_\alpha = \frac{1}{4} n_\alpha u_{T,\alpha}$, where $u_{T,\alpha}$ is the thermal velocity of α.

With a strong magnetic field B (e.g. 0.15 Tesla) parallel to the y direction, the charged species and power losses perpendicular to the magnetic field are significantly reduced. The diffusion coefficient of the plasma perpendicular to the magnetic field can be written as $D_{\perp a} \approx \mu_i T_e/(1 + (\omega_c \tau_e)^2)$, where $\omega_c = eB/m_e$ is the electron cyclotron frequency, m_e is the electron mass, $\tau_e = \lambda_e/\nu_{e,th}$, λ_e is the electron mean free path, $\nu_{e,th} = \sqrt{8eT_e/\pi m_e}$ is the electron thermal velocity. The neutral species losses are not affected by the magnetic field.

The above model is established by the built-in plasma module of the commercial software COMSOL [5]. There are 12 primary species and 21 major reactions considered in the model. The 12 primary species considered are divided into neutral, positive, and negative species. The neutral species consist of Ar, Ar^m,O, O2, O3, and $O_2(a)$. The positive and negative species considered are Ar^+, O^+,O_2^+, O^-,O_2^-, and e. The reactions included in the model are summarized in Table 1. Most of the heavy particle reactions are adopted from the reduced chemistry set provided by Gaens and Bogaerts [8]. In this reduction, only the reactions that contribute to more than 10% to the formation or destruction of a species were selected to reduce the number of reactions. The electron-impact reactions are characterized by the corresponding cross section data. For plasmas with a relatively high pressure used in this model, the electron energy distribution function (EEDF) is assumed as Maxwellian.

2.3. Preparation of bacteria

The bacteria used for this study was *Escherichia coli* and was procured from a ThermoFischer Culti-loop. The bacterial sample was prepared following the given procedure for the indirect (broth) method. The broth used was a Luria-Bertani (LB) broth, recommended for the growth of *E. coli*, prepared in an autoclave. The cultures were grown and kept at 37 °C. After 24 h a serial dilution and dilution plating on LB and agar media petri dishes were performed to calculate the number of bacteria present in each sample. The colonies were counted using Fiji ImageJ software and the Watershed segmentation function [29]. Then 50 μL of the bacterial cell suspension in the LB broth was deposited on sterile glass slides as a droplet using a pipette and a new sterile tip, then left to spread out and dry for no more than 10 min. After they were dry the inoculated glass slides were then placed on a boat inside the plasma tube for treatment.

Each bacterial slide was exposed to plasma treatment times of 10 s, 30 s, 1 min, 1.5 min, and 2.5 min. These treatments varied by pressure, location, and whether a magnetic field was present or not. All the plasma treatments for each round of testing were performed on the same day in order to make sure that the bacterial suspension was the same across each treatment. The experiments were repeated at least three times and for each round of tests, one sample was not exposed to the plasma and was kept as a control.

After the treatment was completed the boat with the inoculated glass slide was extracted. Each slide was swabbed with a new sterile swab. The swab was then mixed into a sterile vial with 10 mL sterilized phosphate-buffered saline (PBS). The swab was then discarded. The inoculated vial with PBS was then mixed and a 50 μL sample was taken using a pipette and new sterile tip. The 50 μL sample was placed on an LB and agar media petri dish and a spread plate was made. The plates and vials were labeled accordingly and left to incubate for ~24 h.

2.4. Optical emission spectroscopy

Optical emission spectroscopy (OES) studies were performed for the different pressures, and with and without a magnetic field to determine the primary plasma species and relative concentrations. OES was performed using an optical spectrometer (USB4000, Ocean Optics, Inc. USA).

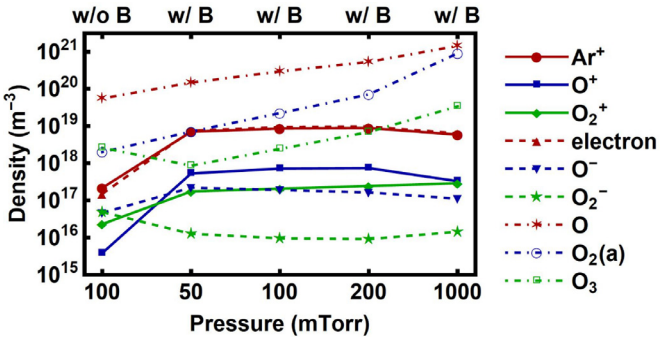

Fig. 2. The number densities of plasma species under 100 mTorr without a magnetic field ***B***, and under pressures from 50 mTorr to 1 Torr with an external magnetic field of 0.15 T. The absorbed power is 70 W in all cases.

3. Results and discussion

3.1. Enhancement of plasma density by a magnetic field

Using the plasma model described above, the magnetic enhancement of the dielectric barrier discharges is verified and proven effective. The number densities of plasma species under different conditions are illustrated in Fig. 2. With an absorbed power of 70 W and 90%-Ar + 10%-O_2 feeding gas, the external magnetic field leads to significantly increased number densities of all charged particles except O^{2-}. However, with the magnetic field, the densities of the charged particles decrease as the pressure increases. This is because the magnetic confinement is weakened under the enhanced electron-neutral collisions. The number densities of neutral species tend to increase by applying an external magnetic field and by increasing the pressure.

Optical emission spectroscopy is then used to confirm that the addition of the magnetic field increases the plasma efficiency. Comparing the intensities at the peaks for plasmas with and without a magnetic field, the addition of the magnetic field increases the intensities by 4–7 times in the direct plasma region and by 2 times in the immediate afterglow region (Fig. 3). These findings are in good agreement with the modeled densities of the excited oxygen species (e.g. O_2(a)), which dominate the optical emissions. In a low density plasma, the neutral molecules surpass the Coulomb interactions of the charged molecules [10]. The charged particles then have a higher probability of colliding with the neutral particles than with other charged particles, which impedes plasma effects [10]. Applying a magnetic field perpendicular to the E-field increases the plasma density by trapping the electrons. This causes increased collisions with the background gas and increased power efficiency [34]. This increase in efficiency allows for the plasma to reach high density without having to increase the power and/or pressure. It is worth noting that the global plasma model only predicts the major species in the bulk plasmas rather than the species distributions in the reactor. The modeling results provide information on what species could play essential roles in the sterilization. The actual concentrations of the interested plasma species at the sample locations are determined from the optical emission measurements.

3.2. Plasma induced sample heating

It has been shown that a temperature of 60 °C is the threshold of E.coli death [24]. Keeping the temperature below 60 °C ensures that polymer-based medical devices will not be heat damaged and that heat is not the mechanism of sterilization [25]. A temperature study is also conducted and repeated three times. The results shown in Fig. 4 depict the average temperature. The maximum uncertainty between the three recorded trials was ± 4 °C. This variation in temperature was mainly due to the measurement by the infrared thermometer and the pointing location in the sample surface. The graph clearly shows that the

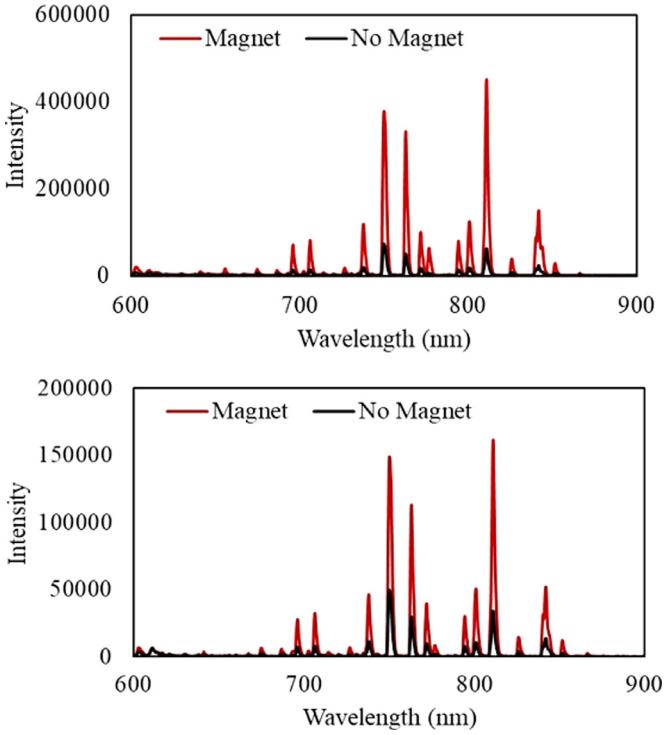

Fig. 3. Top: Intensity of the direct area with and without a magnet at 100 mTorr. Bottom: Intensity of the afterglow area with and without a magnet at 100 mTorr.

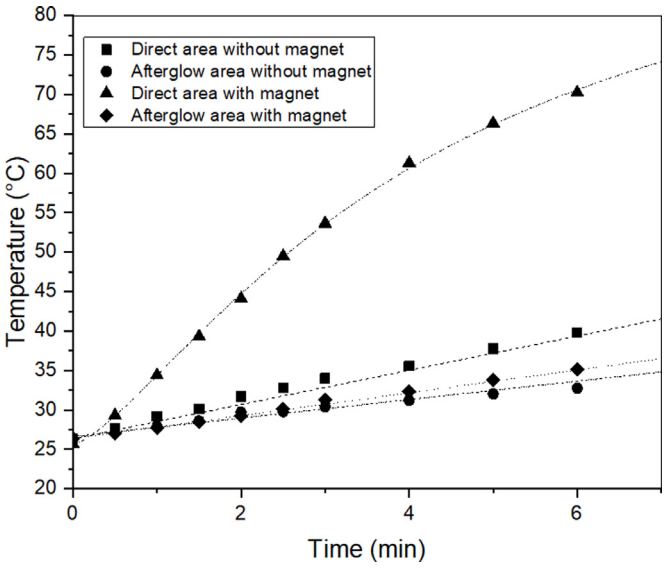

Fig. 4. Temperature comparison between direct and afterglow areas with and without a magnetic field.

temperature within the direct plasma region is higher and increases faster than the afterglow region. After 5 min of treatment at 70 W and ~100 mTorr with a magnetic field, the direct region temperature exceeds the 60 °C threshold. The afterglow region with a magnetic field is much lower in comparison. As will be shown later, the plasma sterilization time needed to reach the SAL for the afterglow region is around 1 min, which implies that the temperature would be well below the threshold for E.coli death. Although the treatments without a magnetic field show a less dramatic temperature difference between the direct and afterglow regions, choosing the afterglow region for treatment position is still more favorable in terms of heating by energetic

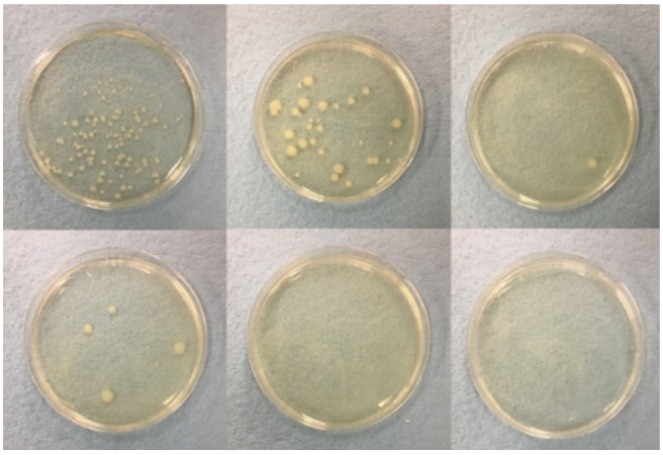

Fig. 5. Growth after sample treatment without magnet. Top from left to right: Control, 10 s, and 30 s. Bottom from left to right: 1 min, 1.5 min and 2.5 min.

charged species to the sample. Comparing the plasma emission intensities and the temperatures of the afterglow region between the treatments with and without a magnetic field highlights that the use of a magnetic field helps to further decrease the temperature of the treatment without compromising the plasma density. Hence, the magnetically enhanced plasma sterilization is expected to be more efficient.

3.3. Effects of a magnetic field on sterilization

Plasma sterilization experiments are first performed without the magnetic field at different times. The plasma discharges are generated at 70 W RF power and ~100 mTorr. The bacterial concentrations were normalized to make them comparable. Fig. 5 shows that there are no visible colonies at 1.5 min. A D-value (decimal reduction time) of 0.113 min is deduced from the survival curve of the treatment. The D-value is the time required to kill 90% of a microorganism population. In order to determine a D-value, a "survivor curve" must be constructed. The survivor curve is created when a population of microorganisms of known number is treated. Samples are taken at different times and the number of surviving microorganisms is determined after incubation [32]. The "survivor curve" is then constructed by plotting the log number of survivors vs. treatment time [32]. Fitting a line to the data allows for the D-value to be calculated from the time required for one logarithm reduction in survivor population or by taking the negative reciprocal of the slope [27]. The D-value is a logarithmic rate of killing and the SAL concept is based on the assumption that exponential first-order kinetics occurs for bacterial inactivation by physical or chemical processes, with a resulting linear inactivation graph on a semi-logarithmic plot [32]. To get SAL compatible sterilization the data needs to be extrapolated based on the results [32]. Using this D-value (0.113 min) the estimated time needed to reach the SAL is 1.57 min, as illustrated in Fig. 6.

Similar experiments are then performed using the same process parameters with an external magnetic field. As discussed before, the external magnetic field efficiently confines high-energy electrons and promote plasma densities and low-temperature treatments in the afterglow region. As shown in Fig. 7, the addition of a magnetic field results in no visible colonies forming at 1 min of treatment. Plotting and analyzing the survival curve of these results (Fig. 6) gives a D-value of 0.069 min. The calculated time needed to reach the SAL is then 0.965 min. Comparing this to the time needed without the magnetic field, the magnetically enhanced plasma decreases treatment time by 61%.

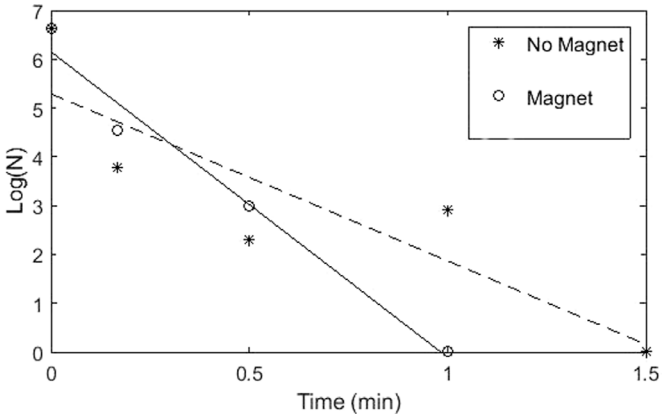

Fig. 6. A comparison between the survival curves of the 100 mTorr treatment with and without a magnetic field.

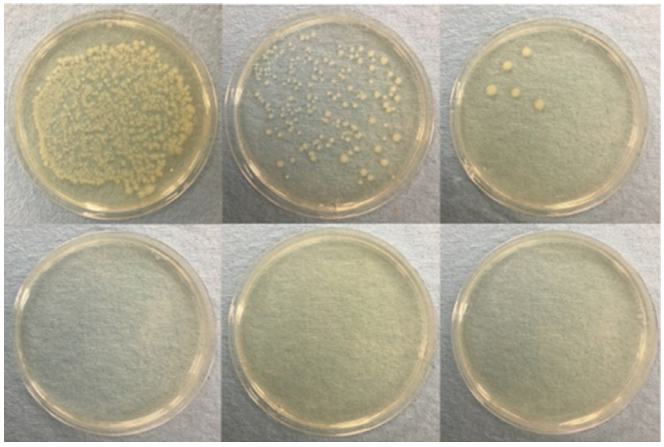

Fig. 7. Growth after sample treatment with a magnet. Top from left to right: Control, 10 s, and 30 s. Bottom from left to right: 1 min, 1.5 min, and 2.5 min.

3.4. Effects of pressure on sterilization

As mentioned in the introduction and illustrated in Fig. 2, the gas pressure has significant effects on the densities of the plasma species. Since the magnetic field promotes the sterilization efficiency, the studies on the effects of gas pressure are performed with a magnetic field and the samples are placed in the afterglow region. From the previous experiments, the pressure of ~100 mTorr results in a D-value of 0.069 min and a SAL of 0.965 min. Subsequently, gas pressures below and above 100 mTorr are studied for comparison. The results are summarized in Table 2. The results indicate that there is an optimal gas pressure ~100 mTorr, which gives the most efficient sterilization. Increasing the gas pressure leads to a rapid increase in the D-value and sterilization time. This is due to the increased frequency of electron-neutral collisions that limit the transfer of sufficient kinetic energy to ionize and excite the gas species. At a lower pressure (e.g. 50 mTorr), the electron-neutral collision probability decreases and subsequently the ionization and excitation are reduced.

3.5. Discussion of sterilization mechanisms

It has been known that reactive oxygen radicals damage the cells by either etching the outer membrane or diffusing through to cause damage to the inner membrane, proteins, and DNA by oxidation [31]. When micro-organisms undergo plasma treatment they are assaulted by the oxygen radicals causing damage that the cell cannot repair [23]. This etching process happens due to the oxygen species being adsorbed onto the surface of the bacteria to react and form volatile compounds.

Table 2
D-value and SAL time at different gas pressures.

Magnetic field	Yes	Yes	Yes	Yes	No
Gas pressure (mTorr)	50	100	200	1000	100
D-value (min)	0.133 ± 0.01	0.069 ± 0.02	0.078 ± 0.02	0.294 ± 0.04	0.113 ± 0.02
SAL time (min)	1.713 ± 0.30	0.965 ± 0.08	1.06 ± 0.08	4.00 ± 0.50	1.57 ± 0.30

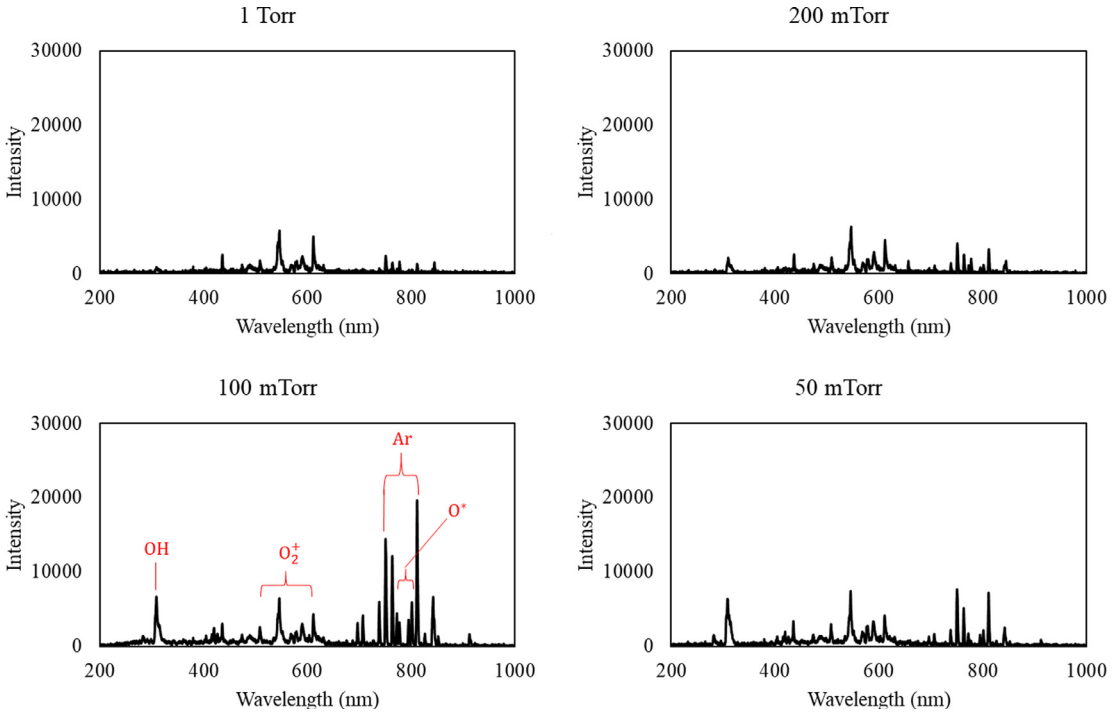

Fig. 8. Optical emission spectrum of the afterglow.

Oxygen plasma has been previously shown to be effective for etching and oxidation [7]. The capability of the atomic oxygen species to oxidize is essential to their ability to sterilize [23].

To further understand the sterilization mechanisms, OES studies are performed for the magnetized O_2/Ar plasmas. Fig. 8 depicts the optical emission spectra for the afterglow area at four pressures: 50 mTorr, 100 mTorr, 200 mTorr, and 1 Torr. The major emission lines include 1) atomic oxygen transition lines at 777 nm and 844 nm, 2) O_2* transition lines within the range of 480–580 nm, 3) Ar lines at 750 nm and 811 nm, and 4) OH lines at 287 and 308 nm. Except for OH radicals, all the other species are predicted by the modeling to be dominant in the plasma.

The atomic oxygen transition lines at 777 nm and 844 nm have the greatest intensity at 100 mTorr [7]. The atomic oxygen line at 777 nm for 100 mTorr is ~4.5x greater than 50 mTorr, and ~2x greater than 200 mTorr and 1 Torr. The 100 mTorr atomic oxygen line at 844 nm is ~3.5x greater than 50 mTorr, and ~2.5x greater than 200 mTorr and 1 Torr. In the afterglow, the optical emission intensities of the O_2* species within the range of 480–580 nm are relatively constant at different pressures. As a result of the combined effect of the oxygen radicals, the sterilization is the most efficient at ~100 mTorr pressure. These findings are in good agreement with a previous study [21]. This mechanism is further reinforced by a study conducted by Liu et al. who find that, in the afterglow zone of an oxygen plasma, oxygen radicals are in high concentration and responsible for sterilization [20].

Yang et al. have studied the sterilization mechanisms of argon plasmas. They find that after treatment cells are eroded and their proteins and nucleic acid leak out [35]. The etching and rupturing of the cell membranes are due to argon ion bombardments [35]. These findings, along with the OES results showing that the argon emission peak at 750 nm has the greatest intensity at 100 mTorr, suggest that Ar ion etching also plays a significant role in plasma sterilization. Samples placed in the direct area run the risk of surface damage due to the impact of positive ions through a sheath of relatively high potential [21]. Hence, the afterglow area is a suitable choice for sterilization sample placement.

The UV emission lines at 287 and 308 nm are caused by the transitions of the OH band [28]. There are two possible reasons to form the OH species: 1) the reactions between the oxygen species and the bacteria [33], and 2) the presence of residual H_2O [14]. Since the OH peaks are more intensive at 100 mTorr than at the other pressures in the afterglow, UV radiation highly likely plays a role in sterilization or is an indication of oxygen plasma etching of the bacteria.

4. Conclusion

Plasmas of oxygen and argon mixture have been shown to be able to kill the *E. coli* and the effectiveness depends strongly on the plasma characteristics and gas pressure. A magnetized plasma greatly shortens the sterilization time due to the increased concentrations of the reactive species. The direct discharge region possesses higher plasma density and subsequently leads to more intensive etching and heating that could potentially damage the surfaces of the medical devices under sterilization. Hence, the afterglow region is a preferred location for the samples. The plasma species that contribute to the sterilization include atomic and molecular oxygen radicals (ions and excited species) and argon ions. The work of Berney et al. demonstrates that the sensitivity of E.coli certain UV light is influenced by the specific growth rate [2]. In

order to better evaluate the role of UV radiation of the plasma in killing the bacteria, the specific growth rate should be measured and further evaluated to quantify its effects in sterilization.

Declaration of Competing Interest

None

Acknowledgements

The authors would like to thank the National Science Foundation for its support (Grant No. 1700785 and 1700787).

References

[1] S. Ashida, C. Lee, M.A. Lieberman, Spatially averaged (global) model of time modulated high density argon plasmas, Journal of Vacuum Science & Technology A: Vacuum, Surfaces, and Films 13 (5) (1995) 2498–2507, https://doi.org/10.1116/1.579494.

[2] M. Berney, H.-.U. Weilenmann, J. Ihssen, C. Bassin, T. Egli, Specific growth rate determines the sensitivity of escherichia coli to thermal, UVA, and solar disinfection, Appl. Environ. Microbiol. 72 (4) (2006) 2586–2593, https://doi.org/10.1128/AEM.72.4.2586-2593.2006.

[3] A. Bogaerts, Effects of oxygen addition to argon glow discharges: A hybrid monte carlo-fluid modeling investigation, Spectrochimica Acta. Part B: Atomic. Spectroscopy 64 (11–12) (2009) 1266–1279, https://doi.org/10.1016/J.SAB.2009.10.003.

[4] A.A. Bol'shakov, B.A. Cruden, R. Mogul, M.V. V.S. Rao, S.P. Shama, B.N. Khare, M. Meyyappan, Radio-Frequency oxygen plasma as a sterilization source, AIAA Journal 42 (4) (2004) 823–832, https://doi.org/10.2514/1.9562.

[5] COMSOL Multiphysics 5.3, Plasma Module User's Guide, COMSOL Inc, Stockholm, 2017.

[6] P.C. Cosby, Electron-impact dissociation of oxygen, J. Chem. Phys. 98 (12) (1993) 9560–9569, https://doi.org/10.1063/1.464387.

[7] U. Cvelbar, N. Krstulović, S. Milošević, M. Mozetič, Inductively coupled RF oxygen plasma characterization by optical emission spectroscopy, Vacuum 82 (2 SPEC. ISS.) (2007) 224–227, https://doi.org/10.1016/j.vacuum.2007.07.016.

[8] W.Van Gaens, A. Bogaerts, Kinetic modelling for an atmospheric pressure argon plasma jet in humid air, J. Phys. D. Appl. Phys. (2013), https://doi.org/10.1088/0022-3727/46/27/275201.

[9] J.T. Gudmundsson, E.G. Thorsteinsson, Oxygen discharges diluted with argon: dissociation processes, Plasma Sources Science and Technology 16 (2) (2007) 399–412, https://doi.org/10.1088/0963-0252/16/2/025.

[10] Inan, U., & Gołkowski, M. (2010). Principles of plasma physics for engineers and scientists plasma paper 2018. Retrieved fromhttps://books.google.com/books?hl=en&lr=&id=kFRJ9AT9BE0C&oi=fnd&pg=PR1&ots=bNBaBqqEmA&sig=lIIBL9Wzk2KNY3PR8OvjTMdVBXc.

[11] Y. Itikawa, A. Ichimura, K. Onda, K. Sakimoto, K. Takayanagi, Y. Hatano, ... S. Tsurubuchi, Cross sections for collisions of electrons and photons with oxygen molecules, J. Phys. Chem. Ref. Data 18 (1) (1989) 23–42, https://doi.org/10.1063/1.555841.

[12] Yukikazu Itikawa, Cross sections for electron collisions with oxygen molecules, J. Phys. Chem. Ref. Data 38 (1) (2009) 1–20, https://doi.org/10.1063/1.3025886.

[13] F. Kannari, M. Obara, T. Fujioka, An advanced kinetic model of electro-n-beam-excited KrF lasers including the vibrational relaxation in KrF*(b) and collisional mixing of KrF*(b, C), J. Appl. Phys. 57 (9) (1985) 4309–4322, https://doi.org/10.1063/1.334590.

[14] N. Krstulović, I. Labazan, S. Milošević, U. Cvelbar, A. Vesel, M. Mozetič, Optical emission spectroscopy characterization of oxygen plasma during treatment of a PET foil, J. Phys. D. Appl. Phys. 39 (17) (2006) 3799–3804, https://doi.org/10.1088/0022-3727/39/17/014.

[15] M.S. Kyi, J. Holton, G.L. Ridgway, Assessment of the efficacy of a low temperature hydrogen peroxide gas plasma sterilization system, J. Hosp. Infect. 31 (4) (1995) 275–284 Retrieved from https://www.sciencedirect.com/science/article/pii/0195670195902066.

[16] R.R. Laher, F.R. Gilmore, Updated excitation and ionization cross sections for electron impact on atomic oxygen, J. Phys. Chem. Ref. Data 19 (1) (1990) 277–305, https://doi.org/10.1063/1.555872.

[17] M.-.H. Lee, C.-.W. Chung, Self-consistent global model with multi-step ionizations in inductively coupled plasmas, Phys. Plasmas. 12 (7) (2005) 073501, , https://doi.org/10.1063/1.1935407.

[18] Lerouge, S., & Simmons, A. (2012). Sterilisation of biomaterials and medical devices plasma paper 2018. Retrieved fromhttps://books.google.com/books?hl=en&lr=&id=xVtEAgAAQBAJ&oi=fnd&pg=PP1&ots=AEZnRWR3q-&sig=jC8kCOdriZGGeNcxM5X73oLAVHY.

[19] M.A. Lieberman, A. Michael, A.J. Lichtenberg, Principles of Plasma Discharges and Materials Processing, Wiley-interscience, 2005.

[20] H. Liu, J. Chen, L. Yang, Y. Zhou, Long-distance oxygen plasma sterilization: Effects and mechanisms, Appl. Surf. Sci. 254 (6) (2008) 1815–1821, https://doi.org/10.1016/J.APSUSC.2007.07.152.

[21] M. Moisan, J. Barbeau, S. Moreau, J. Pelletier, M. Tabrizian, L. Yahia, Low-temperature sterilization using gas plasmas: a review of the experiments and an analysis of the inactivation mechanisms, Int. J. Pharm. 226 (1–2) (2001) 1–21, https://doi.org/10.1016/S0378-5173(01)00752-9.

[22] Michel Moisan, K. Boudam, D. Carignan, D. Kéroack, P. Levif, J. Barbeau, ... W. Zorzi, Sterilization/disinfection of medical devices using plasma: the flowing afterglow of the reduced-pressure N 2 -O 2 discharge as the inactivating medium, The European Physical Journal Applied Physics 63 (1) (2013) 10001, https://doi.org/10.1051/epjap/2013120510.

[23] M. Moreau, N. Orange, M.G.J. Feuilloley, Non-thermal plasma technologies: New tools for bio-decontamination, Biotechnology Advances. (2008), https://doi.org/10.1016/j.biotechadv.2008.08.001.

[24] T. Ohshima, K. Okuyama, M. Sato, Effect of culture temperature on high-voltage pulse sterilization of escherichia coli, J. Electrostat. 55 (3–4) (2002) 227–235, https://doi.org/10.1016/S0304-3886(01)00206-6.

[25] N. Philip, B. Saoudi, M.-.C. Crevier, M. Moisan, J. Barbeau, J. Pelletier, The respective roles of UV photons and oxygen atoms in plasma sterilization at reduced gas pressure: the case of N/sub 2/-O/sub 2/ mixtures, IEEE Transactions on Plasma Science 30 (4) (2002) 1429–1436, https://doi.org/10.1109/TPS.2002.804203.

[26] W.A. Rutala, M.F. Gergen, D.J Weber, Sporicidal activity of a new low-temperature sterilization technology: the sterrad 50 sterilizer, Infection Control & Hospital Epidemiology the Official Journal of the Society of Hospital Epidemiologists of America 20 (7) (1999) 514–516, https://doi.org/10.1086/501662.

[27] E.R. Sanders, Aseptic laboratory techniques: plating methods, Journal of Visualized Experiments JoVE (63) (2012) e3064, https://doi.org/10.3791/3064.

[28] A. Sarani, A.Y. Nikiforov, C. Leys, Atmospheric pressure plasma jet in Ar and Ar/h2o mixtures: Optical emission spectroscopy and temperature measurements, Phys. Plasmas. 17 (6) (2010) 063504, , https://doi.org/10.1063/1.3439685.

[29] J. Schindelin, I. Arganda-Carreras, E. Frise, V. Kaynig, M. Longair, T. Pietzsch, ... A. Cardona, Fiji: an open-source platform for biological-image analysis, Nat. Methods 9 (7) (2012) 676–682, https://doi.org/10.1038/nmeth.2019.

[30] H. Shintani, A. Sakudo, P. Burke, G. McDonnell, Gas plasma sterilization of microorganisms and mechanisms of action, Exp. Ther. Med. 1 (5) (2010) 731–738, https://doi.org/10.3892/etm.2010.136.

[31] A. Sureshkumar, R. Sankar, M. Mandal, S. Neogi, Effective bacterial inactivation using low temperature radio frequency plasma, Int. J. Pharm. 396 (1–2) (2010) 17–22, https://doi.org/10.1016/J.IJPHARM.2010.05.045.

[32] T. von Woedtke, A. Kramer, K.-.D. Weltmann, Plasma sterilization: What are the conditions to meet this claim? Plasma. Processes and Polymers 5 (6) (2008) 534–539, https://doi.org/10.1002/ppap.200800013.

[33] D. Vujošević, M. Mozetič, U. Cvelbar, N. Krstulović, S. Milošević, Optical emission spectroscopy characterization of oxygen plasma during degradation of escherichia coli, J. Appl. Phys. 101 (10) (2007) 103305, , https://doi.org/10.1063/1.2732693.

[34] K. Wang, B. Zheng, M. Shrestha, T. Schuelke, Q.H. Fan, Magnetically enhanced plasma exfoliation of polyaniline-modified graphene for flexible solid-state supercapacitors, Energy Storage Materials 14 (2018) 230–237, https://doi.org/10.1016/j.ensm.2018.04.004.

[35] L. Yang, J. Chen, J. Gao, Low temperature argon plasma sterilization effect on pseudomonas aeruginosa and its mechanisms, J. Electrostat. 67 (4) (2009) 646–651, https://doi.org/10.1016/j.elstat.2009.01.060.